Bounded dam-break flows with tailwaters

Alexander J. N. Goater and Andrew J. Hogg†

Centre for Environmental and Geophysical Flows, School of Mathematics, University of Bristol,
University Walk, Bristol BS8 1TW, UK

The gravitationally driven collapse of a reservoir into an initially stationary layer of fluid, termed the tailwater, is studied using the nonlinear shallow water equations. The motion is tackled using the hodograph transformation of the governing equation which allows the solutions for velocity and depth of the shallow flowing layer to be constructed by analytical techniques. The front of the flow emerges as a bore across which the depth of the fluid jumps discontinuously to the tailwater depth. The speed of the front is initially constant, but progressively slows once the finite extent of the reservoir begins to influence the motion. There then emerges a variety of phenomena depending upon the depth of the tailwater relative to the initial depth of the reservoir. Provided that the tailwater is sufficiently deep, a region of quiescent fluid emerges adjacent to the rear wall of the reservoir, followed by a region within which the velocity is negative. Also it is shown that for non-vanishing tailwater depths, continuous solutions for the velocity and height of the flowing layer breakdown after a sufficient period and develop an interior bore, the location and time of inception of which are calculated directly from quasi-analytical solutions.

1. Introduction

The instantaneous removal of a dam that confines a reservoir of fluid generates an unsteady and spatially evolving motion as the fluid gravitationally slumps downstream. This dam-break flow has many direct engineering applications (e.g. Valiani, Caleffi & Zanni 2002) and has been studied for many years. Ritter (1892) derived an analytical solution for the dam-break flow of an infinite volume of fluid over a dry bed with no resistance, and this was extended by Stoker (1957) to flow over a wet horizontal plane from an unbounded reservoir. More recently, the complete analytical solution for the inviscid collapse of a bounded reservoir over a dry bed was presented by Hogg (2006). In this study we develop the analytical solution for a dam-break flow of a finite reservoir into a tailwater, defined here as the layer of quiescent fluid ahead of the gravitationally driven collapse of fluid, and we show that the presence of the tailwater introduces a number of interesting differences to the ensuing motion.

The failure of dams and the resulting flows can cause substantial damage to property and loss of life; recent disasters include the Big Bay Dam, Mississippi, USA in March 2004 (Yochum, Goertz & Jones 2008), the Qixianhu Dam, Yunnan, China

† Email address for correspondence: a.j.hogg@bristol.ac.uk

in July 2005 (He, Wang & Huang 2008) and the Kolontár dam failure, Hungary in October 2010 (Enserink 2010). Predictions for dam-break flows are typically found using numerical simulations (Shigematsu, Liu & Oda 2004), however computational models can often struggle to resolve the front of the motion due to steep gradients and diminishing heights resulting in numerical instabilities or significant errors. Thus, obtaining complete analytical solutions, as presented here, is important for verification of these models, particularly those that employ a very shallow tailwater. More generally, new numerical schemes are often tested with dam-break simulations (e.g. Macchione & Morelli 2003) due to the aforementioned difficulties that can arise at the front of the motion and to the availability of analytical solutions (Ritter 1892; Stoker 1957) against which to test them. Here we have found another complete analytical solution to a dam-break problem that offers a test case for numerical schemes that integrate the governing equations and that leads to some different phenomena from what is found in other solutions.

There have been relatively few comprehensive experimental studies of the release of a finite reservoir of fluid into a tailwater experimentally beyond the time at which the rear wall begins to influence the motion. Stansby, Chegini & Barnes (1998) performed experiments to analyse the initial formation of the bore at the front of a dam break flow with a tailwater and found reasonable agreement to analytical results of Stoker (1957). However, the length of the channel ahead of the lock was considerably shorter than the length of the lock and thus only early time analytical solutions for which the finite length of the lock is immaterial are necessary for comparison. Similarly, Leal, Ferreira & Cardoso (2006) compared experimental data from a range of sources for the speed at the front of these flows immediately after the removal of the lock gate and also found good agreement with Stoker (1957) during this initial phase. The experiments conducted by Jánosi *et al.* (2004) were within a channel that was significantly longer than the length of the lock and were not terminated at the point at which the finite extent of the lock influenced the motion. Hence, they are suitable for comparison with the results presented within this study and at the end of this paper (§ 7) we show reasonable agreement between the new theoretical predictions and these experimental results.

In this study we model the two-dimensional motion using the nonlinear shallow water equations on the assumption that resistive and dispersive effects are negligible (Peregrine 1971). These coupled governing equations are hyperbolic and this permits the identification of characteristic variables. Subsequent interchange of the dependent and independent variables (the hodograph transformation) then renders the governing equations linear and this permits more readily the construction of the flow field from the initial conditions. This technique has been used by Carrier & Greenspan (1957) and Carrier, Wu & Yeh (2003) to study the run-up of nonlinear waves on a beach, by Kerswell (2005) to analyse the frictional collapse of a granular column, by Dressler (1958) and Ancey *et al.* (2008) to capture the gravitational slumping of inviscid fluid on a sloping boundary and by Pritchard, Guard & Baldock (2008), Antuono & Hogg (2009) and Hogg, Baldock & Pritchard (2010) to reveal aspects of the dynamics of swash and beach overtopping. However perhaps the closest study to this one is that of Hogg (2006) in which a dam-break flow of finite extent is modelled as it gravitationally slumps into an initially dry domain. The general methodology that underlies all of these studies is to exploit the characteristic structure of the governing equations and in particular to use the hodograph transformation to assist in constructing the solutions in regions where both characteristics vary. This relies upon an invertible relationship between dependent and independent variables and the absence of discontinuities in the solutions. Of course the nonlinear shallow water

equations may form discontinuous solutions ('bores'), see Stoker (1957) for example, and this requires a more careful application of the hodograph techniques (Hogg 2006; Antuono & Hogg 2009).

Part of our motivation for employing these quasi-analytical techniques is that the flow solutions that arise exhibit a rich structure that may be difficult to elucidate directly from purely numerical integration of the governing equations. Here we identify three novel dynamical features that arise due to the presence of the tailwater and which do not occur from dam-break slumps into an initially dry domain. First we find that the front of the flow, here defined as the foremost downstream location at which the fluid is in motion, initially moves with constant speed (cf. Stoker 1957) for some period but then decelerates. Next we establish that after a sufficient time following release and for flows with tailwater depths in excess of a determined value, there is a region of motionless fluid adjacent to the rear wall with depths less than the tailwater. This leads to an evolving region of backwards flow close to the back wall, while the foremost regions of the motion continue to flow forwards. Finally we determine that for all tailwater depths the motion develops an interior bore at some late time following release.

The nonlinear shallow water equations employed in this study neglect dispersive effects. Peregrine (1966) argued that dispersive terms leading to the formation of an undular bore are significant when the difference between the depth of fluid within the dam and within the tailwater is sufficiently small. This is supported by experimental evidence, performed first by Favre (1935) and more recently by Treske (1994) and Soares Frazao & Zech (2002), where it was found that for the release of fluid from behind a lockgate of height h_0 into an initially stationary reservoir of height h_1 an undular bore is formed when $h_1 > 0.72 h_0$ and this indicates that dispersive effects are non-negligible. Despite this, shock conditions that conserve mass and momentum across a discontinuous jump in the fluid depth can be employed to link the conditions at the rear to those at the front of this dispersive region (Whitham 1974). Therefore, the features identified by the non-dispersive shallow water equations may still be found if the dispersive region is sufficiently small relative to the streamwise length scale of the rest of the flow. In what follows, most of the analysis and all of the transitions between different phenomena occur for $h_1 < 0.72 h_0$ and thus we anticipate that dispersive effects do not play a significant role in the dynamics that we describe.

Our paper is structured as follows: first we introduce the model, identify the sole dimensionless parameter that measures the depth of the tailwater relative to the initial depth of the reservoir and we present the hodograph transformation (§ 2). We then exploit the characteristic structure of the underlying equations to develop the initial flow solutions (§ 3). These reproduce the results of Stoker (1957), but additionally show the initial effects of the bounded reservoir. In § 4 we calculate how the front is decelerated, an effect that is reliant upon the effects of the no flow condition at the rear wall of the reservoir influencing the motion. This deceleration then subsequently affects the internal velocity and height fields. We show in § 5 that for some tailwater depths there emerges a motionless region adjacent to the rear wall and thereafter there may be a region of negative velocity. Finally, we demonstrate that after a sufficiently long period of time that depends upon the tailwater depth that all of the flows develop an internal shock (§ 6). Finally we summarize the results, draw some conclusions and compare our theoretical predictions with experimental observations (§ 7). There is also an Appendix in which we give a lengthy algebraic expression that determines when the flows develop an internal shock for some values of the tailwater.
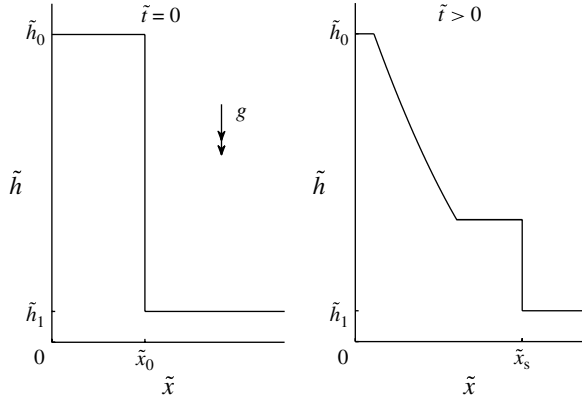
FIGURE 1. Initial configuration of the dam and tailwater at $\tilde{t} = 0$ and a typical height profile at some time after release for $\tilde{t} > 0$. $\tilde{x}_s(\tilde{t})$ denotes the position of the forward propagating shock and marks the front of the moving fluid.

2. Formulation

The initial configuration of this problem is a layer of fluid of height $\tilde{h}_0$ between an impermeable wall at $\tilde{x} = 0$ and a lockgate at $\tilde{x} = \tilde{x}_0$, and a semi-infinite layer of fluid of height $\tilde{h}_1$ in the region $\tilde{x} > \tilde{x}_0$ with $\tilde{h}_0 > \tilde{h}_1$ (see figure 1). Initially, all fluid is at rest before the instantaneous removal of the lockgate at $\tilde{t} = 0$. Thereafter, the fluid flows predominantly horizontally over the underlying boundary; the front of the motion is at $\tilde{x} = \tilde{x}_s(\tilde{t})$ and fluid ahead of this point remains at rest.

We model the fluid motion by the nonlinear shallow water equations on the assumption that the flow is predominantly horizontal and the pressure hydrostatic, (see Peregrine 1971). Denoting the height and horizontal velocity of the flow by $\tilde{h}$ and $\tilde{u}$, respectively, and the gravitational acceleration by g, the shallow water equations are given by

$$\frac{\partial \tilde{h}}{\partial \tilde{t}} + \frac{\partial (\tilde{u}\tilde{h})}{\partial \tilde{x}} = 0 \quad \text{and} \quad \frac{\partial \tilde{u}}{\partial \tilde{t}} + \tilde{u}\frac{\partial \tilde{u}}{\partial \tilde{x}} + g\frac{\partial \tilde{h}}{\partial \tilde{x}} = 0. \tag{2.1}$$

Non-dimensionalizing using

$$h = \frac{\tilde{h}}{\tilde{h}_0}, \quad x = \frac{\tilde{x}}{\tilde{x}_0}, \quad u = \frac{\tilde{u}}{\sqrt{g\tilde{h}_0}}, \quad t = \frac{\tilde{t}\sqrt{g\tilde{h}_0}}{\tilde{x}_0}, \tag{2.2}$$

we obtain

$$\frac{\partial h}{\partial t} + \frac{\partial (uh)}{\partial x} = 0, \quad \frac{\partial u}{\partial t} + u\frac{\partial u}{\partial x} + \frac{\partial h}{\partial x} = 0, \tag{2.3}$$

and henceforth $h_1 \equiv \tilde{h}_1/\tilde{h}_0$ denotes the dimensionless depth of the tailwater. At the front of the motion, in the region propagating away from the wall, we apply general shock conditions that conserve mass and momentum across the forward propagating shock. Denoting the dimensionless speed of the front by $s = \dot{x}_s$, we generate the

following conditions

$$(u - s)h = -sh_1 \tag{2.4}$$

$$(u - s)^2 h + \tfrac{1}{2}h^2 = s^2 h_1 + \tfrac{1}{2}h_1^2. \tag{2.5}$$

To close this system, at the rear of the dam we apply a no flow condition

$$u = 0 \quad \text{on } x = 0. \tag{2.6}$$

The non-dimensionalized shallow water wave equations can now be put into characteristic form and we find that the characteristic variables are

$$\alpha = u + 2c, \quad \beta = u - 2c, \tag{2.7}$$

with $c = \sqrt{h}$, and that

$$\frac{d\alpha}{dt} = 0 \quad \text{on } \frac{dx}{dt} = u + c \tag{2.8}$$

$$\frac{d\beta}{dt} = 0 \quad \text{on } \frac{dx}{dt} = u - c. \tag{2.9}$$

Henceforth, we shall use hodograph variables where the hodograph transformation is made by setting x and t to each be functions of α and β. The characteristic form of the governing equations becomes

$$\frac{\partial x}{\partial \beta} = \frac{1}{4}(3\alpha + \beta)\frac{\partial t}{\partial \beta} \quad \text{on } \alpha = \text{constant} \tag{2.10}$$

$$\frac{\partial x}{\partial \alpha} = \frac{1}{4}(\alpha + 3\beta)\frac{\partial t}{\partial \alpha} \quad \text{on } \beta = \text{constant}. \tag{2.11}$$

This transformation remains invertible when the Jacobian, J, is finite and non-zero, where J is given by

$$J = \frac{\partial x}{\partial \alpha}\frac{\partial t}{\partial \beta} - \frac{\partial x}{\partial \beta}\frac{\partial t}{\partial \alpha} = \frac{(\beta - \alpha)}{2}\frac{\partial t}{\partial \alpha}\frac{\partial t}{\partial \beta} = -2c\frac{\partial t}{\partial \alpha}\frac{\partial t}{\partial \beta}. \tag{2.12}$$

The characteristic equations (2.10) and (2.11) can be combined to form

$$\frac{\partial^2 t}{\partial \alpha \partial \beta} = \frac{3}{2(\alpha - \beta)}\left(\frac{\partial t}{\partial \alpha} - \frac{\partial t}{\partial \beta}\right). \tag{2.13}$$

Thus, the hodograph transformation has enabled us to form a single linear equation from the nonlinear shallow water wave equations. At the rear of the dam we also have a no flow condition

$$x = 0 \quad \text{on } \alpha + \beta = 0, \tag{2.14}$$

which we apply by treating the problem as symmetric about the line $\alpha + \beta = 0$ in the hodograph plane. This condition of symmetry can be alternatively viewed as assuming that there is a virtual dam break in the domain $x < 0$. This virtual dam break has an initial condition that is the reflection of our problem of interest in the plane $x = 0$. Our governing equations then dictate that the flow will be symmetric about a coordinate frame centred at $x = 0$ and therefore we naturally have that $u = 0$ at $x = 0$ without strictly enforcing this condition.

From Garabedian ([1986](#)), using the linearity of the governing ([2.13](#)), we can find the solution within a region D in terms of boundary integrals

$$\int_{\partial D} \boldsymbol{f} \cdot \mathrm{d}\boldsymbol{x} = 0, \tag{2.15}$$

where $\boldsymbol{f}(a, b; \alpha, \beta) = -V\hat{\boldsymbol{a}} + U\hat{\boldsymbol{b}}$. The integration is around the curve ∂D in the hodograph plane such that $\mathrm{d}\boldsymbol{x} = \mathrm{d}a\hat{\boldsymbol{a}} + \mathrm{d}b\hat{\boldsymbol{b}}$ and

$$U = -\frac{3tB}{2(a-b)} + \frac{B}{2}\frac{\partial t}{\partial b} - \frac{t}{2}\frac{\partial B}{\partial b} \tag{2.16}$$

$$V = \frac{3tB}{2(a-b)} + \frac{B}{2}\frac{\partial t}{\partial a} - \frac{t}{2}\frac{\partial B}{\partial a}. \tag{2.17}$$

In the above expressions, $B(a, b; \alpha, \beta)$ is the Riemann function satisfying the adjoint partial differential equation to ([2.13](#)) given by

$$\frac{\partial^2 B}{\partial a \partial b} + \frac{3}{2(a-b)}\left(\frac{\partial B}{\partial a} - \frac{\partial B}{\partial b}\right) - \frac{3B}{(a-b)^2} = 0, \tag{2.18}$$

subject to the boundary conditions

$$\frac{\partial B}{\partial b} = -\frac{3B}{2(a-b)} \quad \text{on } a = \alpha, \qquad \frac{\partial B}{\partial a} = \frac{3B}{2(a-b)} \quad \text{on } b = \beta, \tag{2.19}$$

and $B(a, b; a, b) = 1$. The Riemann function is given by Garabedian ([1986](#)):

$$B(a, b; \alpha, \beta) = \frac{(a-b)^3}{(a-\beta)^{3/2}(\alpha-b)^{3/2}}F\left[\frac{3}{2}, \frac{3}{2}; 1; \frac{(a-\alpha)(\beta-b)}{(a-\beta)(\alpha-b)}\right] \tag{2.20}$$

where F denotes a hypergeometric function, which when evaluated numerically can be expressed in terms of elliptic integrals.

3. Initial motion: geometry of the characteristic plane

We consider the fluid motion within the characteristic (x, t)-plane and define three types of region, a uniform region, within which α and β are constant; a simple region, within which either α or β is constant; and a complex region, within which α and β vary.

Initially the motion is identical to the instantaneous collapse of a dam of infinite extent into a tailwater of depth h_1 centred at $x = 1$ (Stoker [1957](#)). When the fluid is released there is a rarefaction fan of β-characteristics centred at $x = 1$ that travels toward the rear of the dam in which $\alpha = 2$. This is a simple wave region that we denote by S_1. The lead rearward motion is when $\beta = -2$, due to $u = 0$ and $c = 1$, and is given by the path $x = 1 - t$ (see figure [2](#)). Hence, the rear of the dam first has an influence on the motion when $t = 1$. Within this simple wave region, $-2 \leqslant \beta \leqslant \beta_m$, where β_m is the maximum value of β which is found later. Using ([2.11](#)), we find that this region is composed of β-characteristics that are straight lines and are given by

$$x = 1 + \tfrac{1}{4}(2 + 3\beta)t. \tag{3.1}$$

Emanating from $(x, t) = (1, 0)$, next to S_1, we have a uniform wave region U_1 in which $\alpha = 2$ and $\beta = \beta_m$ (see figure [2](#)). This is bounded on the right by the straight

FIGURE 2. The geometry of the characteristic plane a short time after the release of fluid for a tailwater of dimensionless height 0.1, showing the uniform regions U_1 and U_2, the single wave regions S_1 and S_2 and the complex wave regions C_1 and C_2.

line $x = 1 + st$, where s denotes the velocity of the front of the spreading flow and at which there is a shock where the height jumps discontinuously to the tailwater depth. The variables s and β_m are determined by solving the shock conditions (2.5) after having substituted for u and h in terms of α and β and using that $\alpha = 2$ and $\beta = \beta_m$. Hence, we solve the coupled equations

$$\tfrac{1}{16}(\tfrac{1}{2}(2 + \beta_m) - s)(2 - \beta_m)^2 = -sh_1 \tag{3.2}$$

$$\tfrac{1}{2}(\tfrac{1}{16}(2 - \beta_m)^2 + h_1) = -(\tfrac{1}{2}(2 + \beta_m) - s)s \tag{3.3}$$

with the constraints that $s > 0$ and $s \geqslant \beta_m$, which come from that the shock propagates forwards and the shock cannot travel slower than the fluid behind it. We see that s and β_m vary only with h_1, and the characteristic plane which emerges depends strongly on this height of the tailwater. Leal *et al.* (2006) compared this relationship between s and h_1 with experimental data from a range of sources and we reproduce this analytical relationship in figure 3 along with the dependence of β_m on h_1. Note that the speed of the shock has a minimum of $s = 0.93682$ at $h_1 = 0.336$. The value of β_m decreases monotonically as h_1 increases and, hence, the expansion fan toward the rear of the dam, the simple region S_1, becomes narrower as h_1 increases. In the limit $h_1 \to 1$, $s \to 1$ and we recover the linear wave speed ($s = 1$). As h_1 decreases to zero, s and β_m both tend to 2 and so the uniform region U_1 next to the expansion fan S_1 becomes narrower, ultimately vanishing in the limit $h_1 \to 0$. Thus, in the limit $h_1 \to 0$ we recover the results of Hogg (2006) where it was shown that for a finite dam-break release onto a dry bed, the simple region S_1 is unbounded and uniform region U_1 vanishes.

Once the lead rearward β-characteristic meets the rear of the lock it is reflected and becomes a forward propagating α-characteristic with $\alpha = 2$ emanating from $x = 0$ at $t = 1$, which we derive parametrically as $x_b(\beta)$ and $t_b(\beta)$. Along this curve we

FIGURE 3. The shock speed and the characteristic value β_m as functions of the dimensionless tailwater depth, h_1. The dashed lines indicate asymptotic expansions in the regimes $h_1 \ll 1$ and $|1 - h_1| \ll 1$.

find that

$$\frac{\partial x_b}{\partial \beta} = \frac{1}{4}(6 + \beta)\frac{\partial t_b}{\partial \beta} \tag{3.4}$$

and after Hogg (2006) we have that

$$t_b = \frac{8}{(2 - \beta)^{3/2}} \quad \text{and} \quad x_b = 1 + \frac{2(2 + 3\beta)}{(2 - \beta)^{3/2}}. \tag{3.5}$$

These expressions are valid for $-2 \leqslant \beta \leqslant \beta_m$.

The lead reflected characteristic $(x_b(\beta), t_b(\beta))$ forms a boundary to the simple region S_1 until it is met by the maximum β-characteristic in S_1, upon which $\beta = \beta_m$. This β-characteristic then leaves the expansion fan and forms the boundary of the complex region C_1 that is made up of incoming β-characteristics from S_1 and outgoing α-characteristics that have been reflected from the wall. The boundary of this complex region, along which $\beta = \beta_m$ and α varies, is denoted parametrically by $x_1(\alpha)$ and $t_1(\alpha)$ (see figure 2). We find that

$$t_1(2) = \frac{8}{(2 - \beta_m)^{3/2}} \quad \text{and} \quad x_1(2) = 1 + \frac{2(2 + 3\beta_m)}{(2 - \beta_m)^{3/2}}. \tag{3.6}$$

Thus, in the limit of vanishing tailwater depth ($h_1 \to 0$), for which $\beta_m \to 2$, $t_1(2), x_1(2) \to \infty$, hence the lead reflected characteristic from the rear of the dam does not intersect the moving shock at the front of the motion and S_1 is unbounded (cf. Hogg 2006). This is significant as it implies that for this case the front of the flow is not affected by the presence of the rear wall of the lock.

To find an expression for the characteristics within the first complex region, C_1, we employ integration in the hodograph plane about a rectangle with vertices $(2, -2)$, $(2, \beta)$, (α, β) and $(\alpha, -2)$. For this domain (2.15) becomes

$$0 = \int_{-2}^{\beta} U(2, b; \alpha, \beta) \, db - \int_{2}^{\alpha} V(a, \beta; \alpha, \beta) \, da + \int_{\beta}^{-2} U(\alpha, b; \alpha, \beta) \, db$$

$$- \int_{\alpha}^{2} V(a, -2; \alpha, \beta) \, da. \tag{3.7}$$

We proceed by first integrating by parts the terms containing a derivative of t in the second and third integrals and applying the boundary conditions. Second we integrate by parts the terms containing a derivative of B in the first and last integrals and apply that on $\alpha = -2$, $t = 8/(2 - \beta)^{3/2}$ and by symmetry in the hodograph plane on $\beta = 2$, $t = 8/(2 + \alpha)^{3/2}$. Collecting the remaining terms, applying $B(a, b; a, b) = 1$ and using that $t(2, -2) = 1$ we find

$$t = B(2, -2; \alpha, \beta). \tag{3.8}$$

We can now also obtain the boundary of the complex region $(x_1(\alpha), t_1(\alpha))$ by setting $\beta = \beta_m$, hence we have that $t_1(\alpha) = B(2, -2; \alpha, \beta_m)$ and by integrating along this characteristic we find

$$x_1(\alpha) = x_1(2) + \int_{2}^{\alpha} \frac{1}{4}(\alpha + 3\beta_m) \frac{\partial t_1}{\partial \alpha} \, d\alpha. \tag{3.9}$$

Hogg (2006) showed this first complex region will only be bounded if $\beta_m < 0$. This condition is satisfied here provided that $h_1 > 0.0275$. Hence, dam breaks with a tailwater height that is sufficiently small ($h_1 < 0.0275$) have a complex region next to rear wall that exists for all times after $t = 1$.

We find the trajectory of the lead reflected characteristic (x_b, t_b) as it crosses the uniform region U_1 to meet the shock (see figure 2). In doing so, it forms the boundary between U_1 and a second simple region S_2. This simple region S_2 contains α-characteristics from C_1 with $-\beta_m \leqslant \alpha \leqslant 2$ and constant β-characteristics from U_1 with $\beta = \beta_m$. Along the boundary (x_b, t_b), $\alpha = 2$ and $\beta = \beta_m$, integrating along this characteristic and using that it came from the point $(x_1(2), t_1(2))$ we have

$$x_b = 1 - \frac{4}{(2 - \beta_m)^{1/2}} + \frac{6 + \beta_m}{4} t_b \tag{3.10}$$

and, hence, it intersects the shock at

$$t_2(2) = \frac{16}{(2 - \beta_m)^{1/2}(6 + \beta_m - 4s)} \tag{3.11}$$

$$x_2(2) = 1 + \frac{16s}{(2 - \beta_m)^{1/2}(6 + \beta_m - 4s)}. \tag{3.12}$$

Here $t_2(\alpha)$ and $x_2(\alpha)$ define the β-characteristic formed from the intersection of the shock and the lead reflected characteristic, which forms a boundary between S_2 and a second complex region C_2 (see figure 2). Note that as above we find that as $h_1 \to 0$, $\beta_m \to 2$ and hence $x_2(2)$, $t_2(2) \to \infty$ and so reflected characteristics do not intersect the shock as in Hogg (2006). Also, as $h_1 \to 1$, $\beta_m \to -2$ and $s \to 1$ hence $x_2(2)$, $t_2(2) \to \infty$ and again reflected characteristics do not intersect the shock. In this latter limit we are recover the linear wave speed for both the shock and the

reflected characteristics and hence they never meet. We note also that for $t < t_2(2)$, the propagation of the shock at the front of the motion is given by Stoker (1957), but for $t > t_2(2)$ the motion of the shock differs. Importantly we anticipate that the speed slows, and this is calculated explicitly in the following analysis.

The asymptotic behaviour of $t_2(2)$ and $x_2(2)$ in the limits $h_1 \to 0$ and $h_1 \to 1$ can be found from ascertaining the asymptotic behaviour of β_m and s in these limits. Performing an expansion of (3.2) and (3.3) in h_1 for $h_1 \ll 1$, we find that

$$\beta_m = 2 - 2^{11/4}h_1^{1/4} + o(h_1^{1/4}) \quad \text{and} \quad s = 2 - 2^{7/4}h_1^{1/4} + o(h^{1/4}) \quad \text{for } h_1 \ll 1. \quad (3.13)$$

Inserting these expressions into (3.11) and (3.12) we find that

$$t_2(2) = 2^{-1/8}h_1^{-3/8} + o(h_1^{-3/8}) \quad (3.14a)$$

and

$$x_2(2) = 1 + 2^{7/8}h_1^{-3/8} + o(h_1^{-3/8}) \quad \text{for } h_1 \ll 1. \quad (3.14b)$$

Using the same procedure for $1 - h_1 \ll 1$, we find that

$$\beta_m = -2 + (1 - h_1) + o((1 - h_1)) \quad (3.15a)$$

and

$$s = 1 - \tfrac{1}{8}(1 - h_1) + o((1 - h_1)) \quad \text{for } 1 - h_1 \ll 1, \quad (3.15b)$$

and hence

$$t_2(2) = x_2(2) = \frac{16}{3(1 - h_1)} + o((1 - h)^{-1}) \quad \text{for } 1 - h_1 \ll 1. \quad (3.16)$$

Figure 4 shows the variation of the time and position, $t_2(2)$ and $x_2(2)$, respectively, with the tailwater depth. We reiterate that these are the times and positions when the speed of the front first deviates from the infinite lock result of Stoker (1957). We note that there is a local minimum in each of the figures with the minimum time that the shock is intersected being $t_2(2) = 6.6470$ when $h_1 = 0.105$ and the minimum position that the shock is intersected being $x_2(2) = 7.4833$ when $h_1 = 0.141$. The asymptotic relations found above are plotted in figure 4 as dashed lines.

We now proceed to find the β-characteristic $(x_2(\alpha), t_2(\alpha))$ that forms the boundary between S_2 and C_2, which emanates from the point at which the shock is met by the lead reflected characteristic. On $(x_2(\alpha), t_2(\alpha))$ $\beta = \beta_m$ and hence it satisfies

$$\frac{\partial x}{\partial \alpha} = \frac{1}{4}(\alpha + 3\beta_m)\frac{\partial t}{\partial \alpha} \quad (3.17)$$

and the α-characteristics that meet it satisfy

$$x_2 = x_1 + \tfrac{1}{4}(3\alpha + \beta_m)(t_2 - t_1). \quad (3.18)$$

Substituting for x_2 in (3.17), we have

$$\frac{\partial x_1}{\partial \alpha} + \frac{3}{4}(t_2 - t_1) + \frac{1}{4}(3\alpha + \beta_m)\left(\frac{\partial t_2}{\partial \alpha} - \frac{\partial t_1}{\partial \alpha}\right) = \frac{1}{4}(\alpha + 3\beta_m)\frac{\partial t_2}{\partial \alpha}. \quad (3.19)$$

Given that x_1 is a β-characteristic with $\beta = \beta_m$, we can substitute for $\partial x_1/\partial \alpha$ in terms of $\partial t_1/\partial \alpha$ to give

$$\frac{1}{4}(\alpha + 3\beta_m)\frac{\partial t_1}{\partial \alpha} + \frac{3}{4}(t_2 - t_1) + \frac{1}{4}(3\alpha + \beta_m)\left(\frac{\partial t_2}{\partial \alpha} - \frac{\partial t_1}{\partial \alpha}\right) = \frac{1}{4}(\alpha + 3\beta_m)\frac{\partial t_2}{\partial \alpha}. \quad (3.20)$$
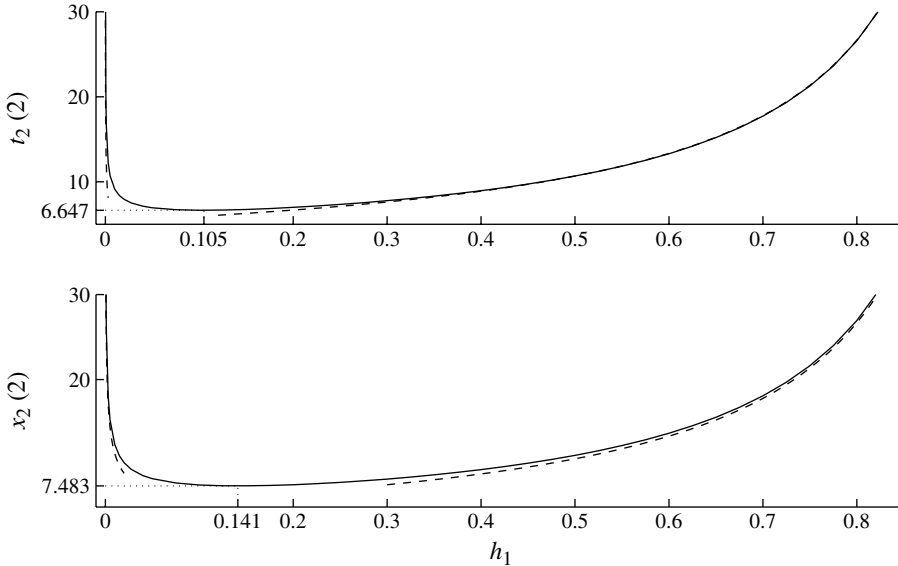
FIGURE 4. The time, $t_2(2)$, and position, $x_2(2)$, of the intersection between the shock and the lead reflected characteristic as a function of the dimensionless tailwater depth h_1. After these times and positions the speed of the frontal shock is diminished. Note that a truncated horizontal scale is employed due to divergence as $h_1 \to 1$, the dashed lines indicate the asymptotic expansions found above in the regimes $h_1 \ll 1$ and $|1 - h_1| \ll 1$. The dotted lines indicate the minimum values of $x_2(2)$ and $t_2(2)$ and the values of h_1 at which they occur.

and after rearranging this gives

$$t_2 - t_1 = -\frac{2}{3}(\alpha - \beta_m)\left(\frac{\partial t_2}{\partial \alpha} - \frac{\partial t_1}{\partial \alpha}\right), \tag{3.21}$$

which can be integrated subject to the conditions of $\alpha = 2$, (3.6) and (3.11), to yield

$$t_2(\alpha) = t_1(\alpha) + \frac{8(4s - 2 - 3\beta_m)}{(6 + \beta_m - 4s)(\alpha - \beta_m)^{3/2}}. \tag{3.22}$$

Inserting this into (3.18) gives

$$x_2(\alpha) = x_1(\alpha) + \frac{2(3\alpha + \beta_m)(4s - 2 - 3\beta_m)}{(\alpha - \beta_m)^{3/2}(6 + \beta_m - 4s)}. \tag{3.23}$$

We have identified the geometry of the characteristic plane up to the point at which reflected characteristics from the rear wall meet the shock. The front speed is given by Stoker (1957) as a result of solving shock conditions at the front and the motion at the rear wall immediately after rearward propagating characteristics meet it are given by Hogg (2006). We have identified five regions of the motion, a uniform region U_1, two simple regions S_1 and S_2 and two complex regions C_1 and C_2. The second complex region C_2 is formed at the front of the motion after the shock has been met by reflected characteristics from the rear wall. This region is of importance in determining the future motion as characteristics are reflected back from the shock, altering the front speed and influencing the motion of fluid behind the shock.
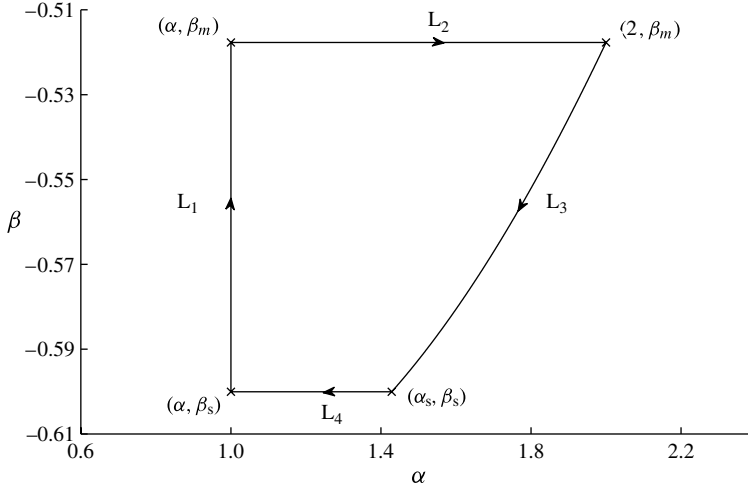
FIGURE 5. The path of the hodograph plane integrals used to solve the time problem in the second complex region for a tailwater of dimensionless height $h_1 = 0.1$, $\alpha = 1$ and $\beta_s = -0.6$.

4. The deceleration of the front: the second complex region C_2

We now calculate the time $t(\alpha, \beta)$ in the second complex region C_2. This complex region is caused by the reflected characteristics from the rear of the dam meeting the shock at the front of the flow, the speed of which is now less than that found earlier from Stoker (1957). In this region we find that $-\beta_m \leqslant \alpha \leqslant 2$ and β is decreasing slowly from the initial value of β_m. The reflected β-characteristics leaving the shock are reflections of the incoming α-characteristics, hence there must be a dependence of β upon α along the shock (see figure 2). Denoting the shock by the hodograph variables α_s, β_s and treating $\beta_s \equiv \beta_s(\alpha_s)$ we employ the boundary integral method used in the first complex region C_1 to find that

$$
\begin{aligned}
0 = & \int_{\beta_s}^{\beta_m} U(\alpha, b; \alpha, \beta) \, \mathrm{d}b - \int_{\alpha}^{2} V(a, \beta_m; \alpha, \beta) \, \mathrm{d}a \\
& + \int_{2}^{\alpha_s} \left(U(a, b(a); \alpha, \beta) \frac{\mathrm{d}b(a)}{\mathrm{d}a} - V(a, b(a); \alpha, \beta) \right) \mathrm{d}a \\
& - \int_{\alpha_s}^{\alpha} V(a, \beta_s; \alpha, \beta) \, \mathrm{d}a.
\end{aligned}
\tag{4.1}
$$

The evaluation of (4.1) entails four line segments, as shown in figure 5. The first is along an α-characteristic from the point at which we want to determine time, (α, β_s), to the boundary of the second complex region formed by a β-characteristic, the point (α, β_m). The second integral is along the β-characteristic with $\beta = \beta_m$, given parametrically by $(x_2(\alpha), t_2(\alpha))$, from the point where it is met by the α-characteristic, (α, β_m), to its origin at the formation of the new shock trajectory, the point $(2, \beta_m)$. The third integral is along the shock trajectory from $(2, \beta_m)$ until we reach the point at which the desired value of β_s is reached, (α_s, β_s). The final integral is along the β-characteristic from the shock at (α_s, β_s) until it meets the point (α, β_s).

Substituting in the definitions for U and V employing integration by parts and the boundary conditions of the Riemann function given by (2.19) we find that

$$t(\alpha, \beta_s) = \frac{1}{2}t(2, \beta_m)B(2, \beta_m; \alpha, \beta_s) + \frac{1}{2}t(\alpha_s, \beta_s)B(\alpha_s, \beta_s; \alpha, \beta_s)$$
$$- \int_\alpha^2 B(a, \beta_m; \alpha, \beta_s)\left(\frac{3t_2}{2(a-b)} + \frac{\partial t_2}{\partial a}\right) da + \int_2^{\alpha_s} \left(-\frac{3t_s B}{2(a-b(a))}(1+b')\right)$$
$$+ \frac{B}{2}\left(b'\frac{\partial t_s}{\partial b} - \frac{\partial t_s}{\partial a}\right) + \frac{t_s}{2}\left(\frac{\partial B}{\partial a} - b'\frac{\partial B}{\partial b}\right) da \tag{4.2}$$

where in second integral $t_s \equiv t(a, b(a))$, $B \equiv B(a, b(a); \alpha, \beta_s)$ and b' is the derivative of $b(a)$ with respect to a.

The second integral in (4.2) entails the time field along the curve (α_s, β_s) as well as the derivatives tangential and perpendicular to the curve. The time $t_s(\alpha_s, \beta_s)$ must be evaluated before the problem can be further progressed and so it is advantageous to remove terms involving its derivatives by integration by parts. To this end, following algebraic manipulations that are similar to those used by Antuono, Hogg & Brocchini (2009), we note that on the shock

$$\frac{dx_s}{da} = s\frac{dt_s}{da}. \tag{4.3}$$

However, from the characteristic (2.10) and (2.11) we find that

$$\frac{dx_s}{da} = \frac{a+b}{2}\frac{dt_s}{da} + \frac{a-b}{4}\left(-\frac{\partial t_s}{\partial a} + b'\frac{\partial t_s}{\partial b}\right), \tag{4.4}$$

where $b = b(a)$, and thus rearranging gives the desired expression

$$-\frac{\partial t_s}{\partial a} + b'\frac{\partial t_s}{\partial b} = \frac{2}{a-b}(2s - (a+b))\frac{dt_s}{da}, \tag{4.5}$$

and hence we can substitute this into (4.2) and use integration by parts to remove the derivative of t_s.

The integral equation (4.2) for $t(\alpha, \beta_s)$ includes the shock speed $s(\alpha)$ and the beta characteristics $\beta_s(\alpha)$ parameterized as functions of α. They may be evaluated directly from the shock conditions (2.5) after substituting for u and h in terms of α and β to give

$$\tfrac{1}{16}(\tfrac{1}{2}(\alpha + \beta) - s)(\alpha - \beta)^2 = -sh_1 \tag{4.6}$$
$$\tfrac{1}{2}(\tfrac{1}{16}(\alpha - \beta)^2 + h_1) = -(\tfrac{1}{2}(\alpha + \beta) - s)s. \tag{4.7}$$

These expressions do not yield explicit forms for β and s. However, in terms of the rotated hodograph co-ordinates given by $\sigma = \alpha - \beta$ and $\lambda = \alpha + \beta$ we find that

$$\tfrac{1}{16}(\tfrac{1}{2}\lambda - s)\sigma^2 = -sh_1 \tag{4.8}$$
$$\tfrac{1}{2}(\tfrac{1}{16}\sigma^2 + h_1) = -(\tfrac{1}{2}\lambda - s)s \tag{4.9}$$

and hence the shock speed s and λ as functions of σ and h_1 are given by

$$s = \sigma\sqrt{\frac{\sigma^2 + 16h_1}{512h_1}} \quad \text{and} \quad \lambda = \frac{2(\sigma^2 - 16h_1)}{\sigma}\sqrt{\frac{\sigma^2 + 16h_1}{512h_1}}. \tag{4.10}$$

Thus, it is convenient to form the second integral in (4.2) in terms of (λ, σ) rather than (α, β); to this end the partial derivatives become

$$\frac{\partial}{\partial \alpha} = \frac{\partial}{\partial \sigma} + \frac{\partial}{\partial \lambda} \quad \text{and} \quad \frac{\partial}{\partial \beta} = -\frac{\partial}{\partial \sigma} + \frac{\partial}{\partial \lambda} \tag{4.11}$$

and denoting $\lambda' \equiv d\lambda/d\sigma$ the total derivatives become

$$\beta' = \frac{\lambda' - 1}{\lambda' + 1} \qquad \frac{dB}{d\alpha} = \frac{dB}{d\sigma} \frac{2}{\lambda' + 1} \qquad \frac{ds}{d\alpha} = \frac{ds}{d\sigma} \frac{2}{\lambda' + 1}. \tag{4.12}$$

Making the change of variables in the second integral of (4.2) and rearranging gives our final result

$$\begin{aligned}
t(\alpha, \beta_s) = {} & t_2(2) B(2, \beta_m; \alpha, \beta_s) \frac{6 + \beta_m - 4s(2)}{2(2 - \beta_m)} \\
& + t(\alpha_s, \beta_s) B(\alpha_s, \beta_s; \alpha, \beta_s) \frac{4s(\alpha_s) - \alpha_s - 3\beta_s}{2(\alpha_s - \beta_s)} \\
& + \int_2^\alpha B(a, \beta_m; \alpha, \beta_s) \left(\frac{3t_2}{2(a - \beta_m)} + \frac{\partial t_2}{\partial a} \right) da \\
& + \int_{2 - \beta_m}^{\sigma_s} t(\tilde{\sigma}, \tilde{\lambda}) \left[B \left(\frac{2\tilde{s} - \tilde{\lambda}}{\tilde{\sigma}^2} - \frac{4\tilde{s}' + \tilde{\lambda}'}{2\tilde{\sigma}} \right) + \frac{\partial B}{\partial \tilde{\sigma}} \left(\frac{\tilde{\lambda}'}{2} - \frac{2\tilde{s} - \tilde{\lambda}}{\tilde{\sigma}} \right) \right. \\
& \left. + \frac{\partial B}{\partial \tilde{\lambda}} \left(\frac{1}{2} - \frac{(2\tilde{s} - \tilde{\lambda})\tilde{\lambda}'}{\tilde{\sigma}} \right) \right] d\tilde{\sigma}, \tag{4.13}
\end{aligned}$$

where in the final integral $B \equiv B((\tilde{\sigma} + \tilde{\lambda})/2, (\tilde{\lambda} - \tilde{\sigma})/2; \alpha, \beta_s)$ and similarly for its derivatives, and $s' \equiv ds/d\sigma$. Before this expression can be used to find the solution throughout the entire complex region C_2, we must first find the time evolution of the shock curve $t_s(\sigma)$. To this end we set $\alpha = \alpha_s$ in (4.13) and changing variables in the first three terms to put everything in terms of σ gives

$$\begin{aligned}
t(\sigma, \lambda) = {} & \frac{2\sigma}{\sigma + 2\lambda - 4s} \left(t_2(2) B \left(2, \beta_m; \frac{\sigma + \lambda}{2}, \frac{\lambda - \sigma}{2} \right) \frac{6 + \beta_m - 4s(2)}{2(2 - \beta_m)} \right. \\
& + \int_2^{(\sigma + \lambda)/2} B \left(a, \beta_m; \frac{\sigma + \lambda}{2}, \frac{\lambda - \sigma}{2} \right) \left(\frac{3t_2}{2(a - \beta_m)} + \frac{\partial t_2}{\partial a} \right) da \\
& + \int_{2 - \beta_m}^{\sigma_s} t(\tilde{\sigma}, \tilde{\lambda}) \left[B \left(\frac{2\tilde{s} - \tilde{\lambda}}{\tilde{\sigma}^2} - \frac{4\tilde{s}' + \tilde{\lambda}'}{2\tilde{\sigma}} \right) + \frac{\partial B}{\partial \tilde{\sigma}} \left(\frac{\tilde{\lambda}'}{2} - \frac{2\tilde{s} - \tilde{\lambda}}{\tilde{\sigma}} \right) \right. \\
& \left. \left. + \frac{\partial B}{\partial \tilde{\lambda}} \left(\frac{1}{2} - \frac{(2\tilde{s} - \tilde{\lambda})\tilde{\lambda}'}{\tilde{\sigma}} \right) \right] d\tilde{\sigma} \right), \tag{4.14}
\end{aligned}$$

where in the final integral

$$B \equiv B \left(\frac{\tilde{\sigma} + \tilde{\lambda}}{2}, \frac{\tilde{\lambda} - \tilde{\sigma}}{2}; \frac{\sigma + \lambda}{2}, \frac{\lambda - \sigma}{2} \right) \tag{4.15}$$

and similarly for its derivatives. This is a Volterra equation of the second kind for $t_s(\sigma)$ and we employ numerical integration and an iterative procedure to find the solution as in Arfken & Weber (1995). This method converges rapidly to the solution, with typically five iterations needed for an accuracy of 10^{-6}. We find that the shock
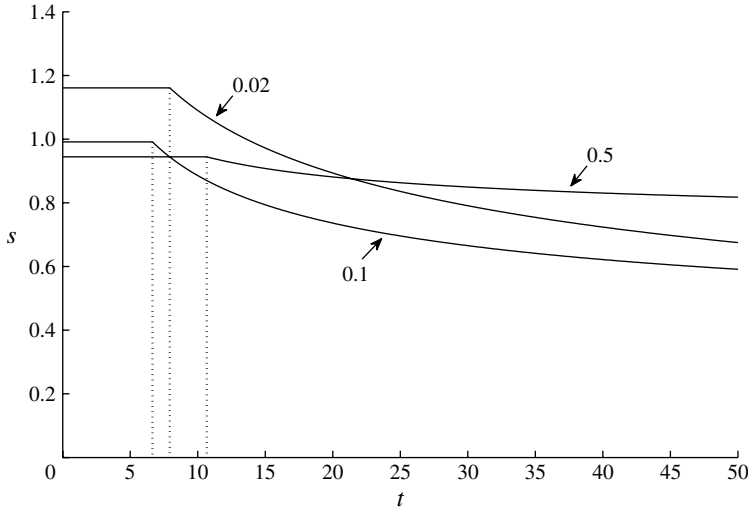
FIGURE 6. The shock speed as a function of time for tailwaters of dimensionless height 0.02, 0.1 and 0.5 as indicated. The dashed lines mark the time at which the shock is met by the lead reflected characteristic and thereafter the speed is progressively reduced.

deviates from its initial path and we see from figure 6 that the speed of the shock s varies continuously after the shock is met by reflected characteristics, supporting this formation of a second complex region rather than another expansion fan.

To find the spatial evolution of the shock, x_s, once it has been met by the first reflected characteristic, we integrate by parts the following expression

$$\frac{\mathrm{d}x_s}{\mathrm{d}\sigma} = s(\sigma)\frac{\mathrm{d}t_s}{\mathrm{d}\sigma} \tag{4.16}$$

to give

$$x_s(\sigma) = x_2(2 - \beta_m) + [s(\sigma)t_s(\sigma)]_{2-\beta_m}^{\sigma} - \int_{2-\beta_m}^{\sigma} t_s\frac{\mathrm{d}s}{\mathrm{d}\sigma}\,\mathrm{d}\sigma \tag{4.17}$$

which we evaluate numerically using the solutions for t_s found from (4.14).

Using the condition that energy must be dissipated across the shock, we require that the shock is always forward propagating and that $u > 0$ at the shock. Therefore, $\lambda = 2u > 0$ and thus $\sigma > 4\sqrt{h_1}$ and $\alpha_s > 2\sqrt{h_1}$ and we have that the reflected characteristics upon which $-\beta_m \leqslant \alpha \leqslant 2\sqrt{h_1}$ never intersect the front. Hence, the second complex region is unbounded and persists for all times after the first reflected characteristic has met the forward propagating shock.

5. The interior velocity and height fields: completing the characteristic plane

5.1. *Unbounded first complex region ($h_1 \leqslant 0.0275$)*

In §3 we found for $h_1 \leqslant 0.0275$ the first complex region C_1 is unbounded and persists for all times. Therefore there is also no boundary to the second simple region S_2 formed by the last rearward propagating characteristic from the lock release reflecting from the rear wall and thus it is also unbounded. From §4 we see that the second complex region will always persist for all times and therefore the characteristic plane for $h_1 \leqslant 0.0275$ is complete. Figure 7 shows the characteristic plane for $h_1 = 0.02$. We
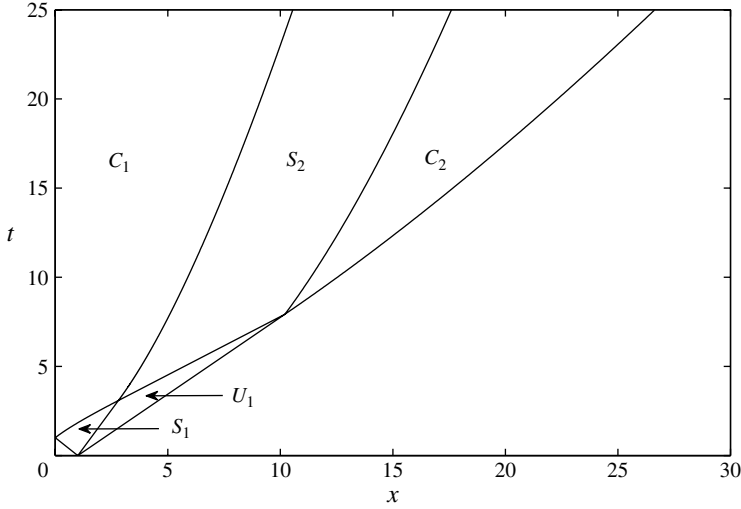
FIGURE 7. Characteristic plane for a tailwater of dimensionless height 0.02.

can clearly see that after the shock is met by reflected characteristics we have three regions of motion, a complex region C_1 next to the rear wall, a complex region C_2 behind the shock and a simple region S_2 between them.

5.2. *Bounded first complex region* ($h_1 > 0.0275$)

Having completed the geometry of the characteristic plane for $h_1 \leqslant 0.0275$ in §5.1 we proceed by considering the case for $h_1 > 0.0275$ in which the first complex region is bounded. The last reflected characteristic from the rear wall forms a boundary between the second simple region, S_2, and a second uniform region, U_2, see figures 2 and 8. Within this second uniform region $\alpha = -\beta_m$ and $\beta = \beta_m$, hence this is a static region in which $u = 0$ and $h = \beta_m^2/4$. Upon the boundary between S_2 and U_2, $\alpha = -\beta_m$ and $\beta = \beta_m$, and it emanates from the point $(0, B(2, -2, -\beta_m, \beta_m))$, hence using (2.10) and denoting the line by (x_3, t_3) we have

$$x_3 = \frac{\beta_m}{2}(B(2, -2, -\beta_m, \beta_m) - t_3). \tag{5.1}$$

This characteristic meets (x_2, t_2) at the point $(x_2(-\beta_m), t_2(-\beta_m))$, and we can calculate the trajectory of (x_2, t_2) after this intersection. Upon being met by this characteristic, (x_2, t_2) becomes a straight line completing the boundary of the second uniform region U_2, with $\alpha = -\beta_m$ and $\beta = \beta_m$ along it. Hence, using (2.11) we have that

$$x_2 = x_2(-\beta_m) + \frac{\beta_m}{2}(t_2 - t_2(-\beta_m)). \tag{5.2}$$

After (x_3, t_3) has met (x_2, t_2) it continues as an α-characteristic forming a boundary between the second complex region C_2 and a third simple region S_3, see figure 8. To find the values of t_3, we substitute $\alpha = -\beta_m$ into (4.13) and the numerically computed values found for t_s. Once we have the time evolution of this α-characteristic, we can find the spatial evolution, x_3, by integrating the characteristic equation (2.10)
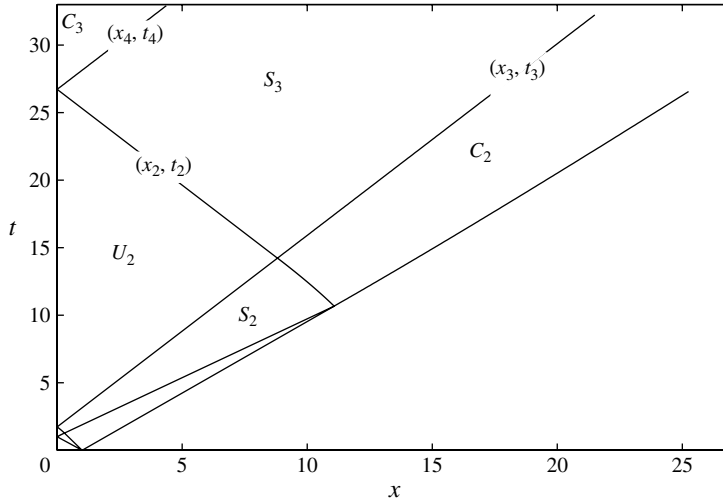
FIGURE 8. Characteristic plane for a tailwater of dimensionless height 0.5.

with $\alpha = -\beta_m$. Using integration by parts the formula for x_3 in this region is

$$x_3 = x_2(-\beta_m) + \left[\frac{1}{4}(-3\beta_m + \beta)t(-\beta_m, \beta)\right]_{\beta_m}^{\beta} + \frac{1}{4}\int_{\beta_m}^{\beta} t(-\beta_m, \beta)\,\mathrm{d}\beta. \qquad (5.3)$$

This can be evaluated numerically using the values found for $t(-\beta_m, \beta)$.

The characteristics reflected from the shock at the front of the motion become β-characteristics that travel back toward the rear wall. The third simple region S_3 is made up entirely of these characteristics and within this region we find that $\alpha = -\beta_m$ and $-2\sqrt{h_1} \leqslant \beta \leqslant \beta_m$. Remarkably, as $\beta \leqslant -\alpha$, the velocity in this entire region is negative.

The lead reflected characteristic from the front, (x_2, t_2), meets the rear wall at the point $(x, t) = (0, t_2(-\beta_m) - (2/\beta_m)x_2(-\beta_m))$. Upon meeting the rear wall it becomes an α-characteristic and forms a boundary between S_3 and a third complex region C_3, see figure 8. This third complex region is composed of β-characteristics that are travelling rearwards from the shock and α-characteristics that are formed from the reflected β-characteristics. We denote the boundary between S_3 and C_3 by (x_4, t_4) and the trajectory of this boundary can be calculated in an identical manner to the segment of (x_2, t_2) that forms a boundary between C_2 and S_2, although in this case x_4 and t_4 are parameterized in terms of β and not α. Using that on the boundary (x_4, t_4) we have

$$\frac{\partial x_4}{\partial \beta} = \frac{1}{4}(-3\beta_m + \beta)\frac{\partial t_4}{\partial \beta} \qquad (5.4)$$

and the boundary is met by incoming β-characteristics upon which

$$x_4 = x_3 + \tfrac{1}{4}(-\beta_m + 3\beta)(t_4 - t_3) \qquad (5.5)$$

we can substitute (5.5) into (5.4) and integrate to find t_4. To evaluate the integration constant we use that $t_4(\beta_m) - t_3(\beta_m) = -(2/\beta_m)x_2(-\beta_m)$. Once we have found t_4 we
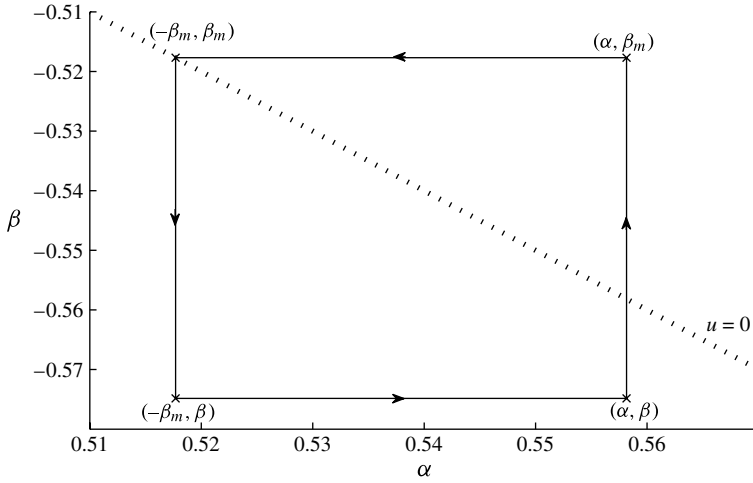
FIGURE 9. An example of the path of the integrals in the hodograph plane used to determine the time field within the third complex region C_3 for $h_1 = 0.1$, $\beta_m = -0.5177$, $\alpha = 0.5582$ and $\beta = -0.5748$.

insert this into (5.5) to find x_4. We find that

$$t_4(\beta) = t_3(\beta) - \frac{2x_2(-\beta_m)}{\beta_m}\left(\frac{2\beta_m}{\beta + \beta_m}\right)^{3/2} \tag{5.6}$$

$$x_4(\beta) = x_3(\beta) - (3\beta - \beta_m)\frac{x_2(-\beta_m)}{2\beta_m}\left(\frac{2\beta_m}{\beta + \beta_m}\right)^{3/2}. \tag{5.7}$$

From (5.6) and (5.7), we see that the boundary (x_4, t_4) does not meet the boundary (x_3, t_3) as $x_2(-\beta_m) > 0$ and we are in the regime of $\beta_m < 0$. Therefore, S_3 is unbounded and we have one final region of motion to determine, a third complex region C_3. This region is composed of incoming β-characteristics from S_3 and α-characteristics formed by the reflected β-characteristics from the rear wall. To find the time evolution in this region we employ integration in the hodograph plane in an identical manner to that used to find the time evolution in the first complex region C_1, where here we integrate around the rectangle with vertices $(-\beta_m, \beta_m)$, $(-\beta_m, \beta)$, (α, β) and (α, β_m), see figure 9. Note that the curve along which $\alpha = -\beta_m$ is given parametrically by $(x_4(\beta), t_4(\beta))$. For this domain (2.15) becomes

$$0 = \int_{\beta_m}^{\beta} U(-\beta_m, b; \alpha, \beta)\, db - \int_{-\beta_m}^{\alpha} V(a, \beta; \alpha, \beta)\, da + \int_{\beta}^{-\beta_m} U(\alpha, b; \alpha, \beta)\, db$$
$$- \int_{\alpha}^{-\beta_m} V(a, \beta_m; \alpha, \beta)\, da. \tag{5.8}$$

Using integration by parts and applying the boundary conditions in an identical manner to that used for C_1 we find that

$$t(\alpha, \beta) = t(-\beta_m, \beta)B(-\beta_m, \beta; \alpha, \beta) - t(-\beta_m, \beta_m)B(-\beta_m, \beta_m; \alpha, \beta)$$
$$+ t(\alpha, \beta_m)B(\alpha, \beta_m; \alpha, \beta)$$
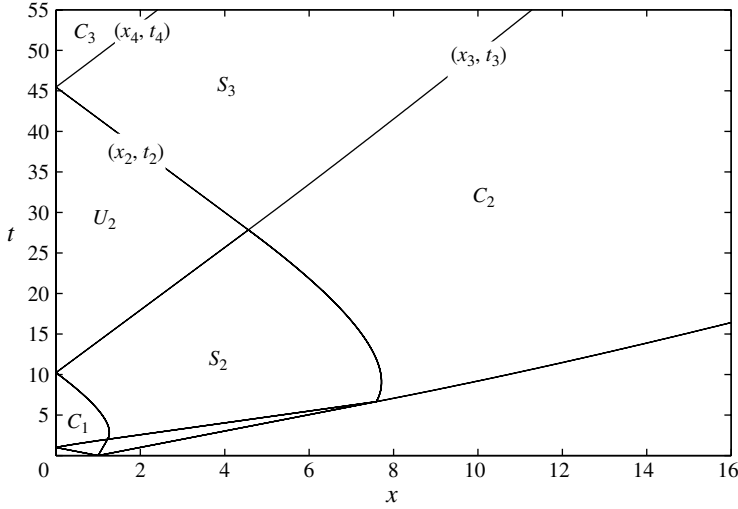
FIGURE 10. Characteristic plane for a tailwater of dimensionless height 0.1.

$$-\int_{\beta_m}^{\beta} t_4(b)\left(\frac{\partial B(-\beta_m, b; \alpha, \beta)}{\partial b} + \frac{3B(-\beta_m, b; \alpha, \beta)}{2(-\beta_m - b)}\right)\mathrm{d}b$$

$$-\int_{\alpha}^{-\beta_m} t_4(-a)\left(\frac{3B(a, \beta_m; \alpha, \beta)}{2(a - \beta_m)} - \frac{\partial B(a, \beta_m; \alpha, \beta)}{\partial a}\right)\mathrm{d}a \qquad (5.9)$$

where t_4 is defined in (5.6). Note that in the second integral $t_4(-a)$ comes from imposing the no flow condition at $x = 0$ by assuming back-to-back dam breaks in an identical manner to that used in the first complex region. The spatial evolution of fluid within C_3 can now be readily found by integrating along a desired β-characteristic and using values found above for the temporal evolution. As the third simple region S_3 is unbounded, β-characteristics from it enter into C_3 for all times and thus C_3 is also unbounded.

We have now completed the geometry of the characteristic plane for all times. Figure 8 shows the characteristic plane computed for a tailwater of height $h_1 = 0.5$. One can identify the various characteristic regions mentioned above, and the slow divergence of the shock from its initial path upon being met by the reflected characteristics from the rear wall. We also construct the characteristic plane for the case where $h_1 = 0.1$ in figure 10. We see that the smaller height of the tailwater has made β_m larger and opened out the first simple and the complex regions. The shock is met by the reflected characteristics at an earlier time.

Once the characteristic structure is completely determined, the height and velocity profiles of the motion can be calculated. This is trivial within the uniform regions, but within the simple and complex regions this entails integration along characteristics to find the position at a given time. Figure 11 shows the height profiles for a tailwater of height 0.1. We can see that the shock at the front of the motion, between the moving fluid and the tailwater, propagates forward with a constant height until the motion from the rear of the dam catches up with it and subsequently the height decreases. Also, we find that the uniform region of constant height forms next to the rear wall, as also shown in figure 10, and within this region $h = \beta_m^2/4 < h_1$ (for $h_1 = 0.1$, we find $\beta_m = -0.5177$, thus $\beta_m^2/4 = 0.0670$). Figure 12 shows the velocity profiles for a
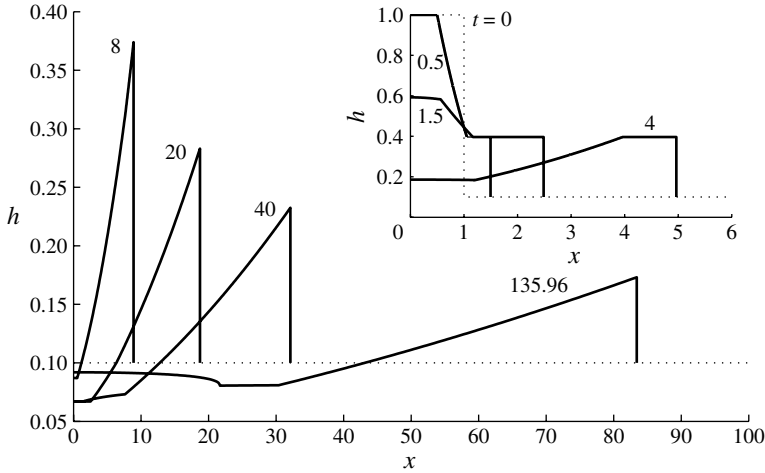
FIGURE 11. The height, $h(x, t)$, as a function of distance for a tailwater of dimensionless height 0.1 at $t = 0.5, 1.5, 4, 8, 20, 40, 135.96$. The dashed line depicts the initial profile at $t = 0$.
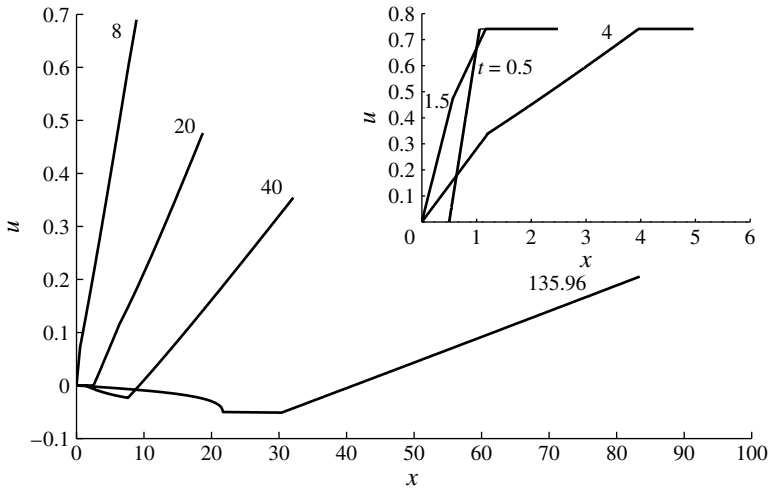
FIGURE 12. The velocity, $u(x, t)$, as a function of distance for a tailwater of dimensionless height 0.1 at $t = 0.5, 1.5, 4, 8, 20, 40, 135.96$.

tailwater of height 0.1. Similarly to the height profiles, we see that the velocity at the front decreases once it has been met by the reflected characteristics from the rear of the dam, which occurs at $t = 6.648$ for $h_1 = 0.1$. At $t = 40$ and $t = 135.96$ we clearly see regions of negative velocity corresponding to S_3 and C_3.

6. The formation of an internal shock

For all tailwater heights we find that eventually an internal shock forms. This is due to the intersection of characteristics and at this point the Jacobian of the hodograph transformation vanishes. Our solution cannot be extended beyond this point without explicitly handling the discontinuity (see, for example, Antuono & Hogg 2009). The

location of the inception of this internal shock varies with the height of the tailwater and is found to lie on three possible boundaries. For tailwater heights sufficiently small, $h_1 \leqslant 0.0513$, the internal shock will be formed along the boundary between C_2 and S_2 due to the intersection of β-characteristics. As the height of the tailwater increases, the value of α at which the shock forms decreases and hence the location of the shock travels along this boundary until it leaves the boundary between C_2 and S_2 and occurs upon the boundary between S_3 and U_2, again due to the intersection of β-characteristics. Increasing the height of the tailwater further, for $h_1 \geqslant 0.0588$, the shock forms upon the boundary between C_3 and S_3 due to α-characteristics intersecting, where these α-characteristics are reflected β-characteristics from the rear wall.

   To find the time at which an internal shock forms on the boundary between C_2 and S_2, we are required to find the value of α for which $\partial t/\partial \beta|_{\beta=\beta_m} = 0$. The complete form of $\partial t/\partial \beta|_{\beta=\beta_m}$ on the boundary between C_2 and S_2 can be found in the Appendix. Once the form of $\partial t/\partial \beta|_{\beta=\beta_m}$ is computed we employ Newton–Raphson root finding to find the value of α for which $\partial t/\partial \beta|_{\beta=\beta_m} = 0$ and then give this value of α, the time and position of the shock formation are given by (3.22) and (3.23), respectively.

   For $0.0513 < h_1 < 0.0588$ the internal shock forms at the boundary between U_2 and S_3. The time of the internal shock formation on this boundary is found by noting that along β-characteristics within S_3

$$x = x_3(\beta) + \tfrac{1}{4}(-\beta_m + 3\beta)(t - t_3(\beta)). \tag{6.1}$$

Differentiating this expression with respect to β and employing the relation that along α-characteristics within S_3

$$\frac{\partial x}{\partial \beta} = \frac{1}{4}(-3\beta_m + \beta)\frac{\partial t}{\partial \beta}, \tag{6.2}$$

and setting $\beta = \beta_m$ we find that the time, t_{shock}, and position, x_{shock}, of shock formation along the boundary between U_2 and S_3 are given by

$$t_{shock} = t_3(\beta_m) + \frac{4}{3}\beta_m \frac{\partial t_3}{\partial \beta}\bigg|_{\beta=\beta_m} \tag{6.3a}$$

$$x_{shock} = x_3(\beta_m) + \frac{2}{3}\beta_m^2 \frac{\partial t_3}{\partial \beta}\bigg|_{\beta=\beta_m}. \tag{6.3b}$$

   For $h_1 \geqslant 0.0588$ the internal shock forms upon the boundary (x_4, t_4) between S_3 and C_3. To find the location of the formation of the shock we must find the value of β for which $\partial t/\partial \alpha|_{\alpha=-\beta_m} = 0$ in the third complex region. Differentiating (5.9) with respect to α and setting $\alpha = -\beta_m$ gives

$$
\begin{aligned}
\frac{\partial t}{\partial \alpha}\bigg|_{\alpha=-\beta_m} &= t(-\beta_m, \beta)\frac{3}{2(\beta_m + \beta)} + t(-\beta_m, \beta_m)\frac{3(-2\beta_m)^{1/2}(\beta - 5\beta_m)}{4(-\beta_m - \beta)^{5/2}} \\
&\quad - t(-\beta_m, \beta_m)\frac{3(-2\beta_m)^{1/2}(\beta - \beta_m)}{2(-\beta_m - \beta)^{5/2}} + \frac{(-2\beta_m)^{3/2}}{(-\beta_m - \beta)^{3/2}}\frac{\partial t(\alpha, \beta_m)}{\partial \alpha}\bigg|_{\alpha=-\beta_m} \\
&\quad - \int_{\beta_m}^{\beta} t_4(b)\frac{-6(\beta_m + \beta)}{8(-\beta_m - b)^{1/2}(-\beta_m - \beta)^{5/2}}\,\mathrm{d}b \\
&\quad + t(-\beta_m, \beta)\left(\frac{3(-2\beta_m)^{1/2}}{2(-\beta_m - \beta)^{3/2}} + \frac{3(-2\beta_m)^{1/2}(3\beta_m + \beta)}{4(-\beta_m - \beta)^{5/2}}\right).
\end{aligned}
\tag{6.4}
$$
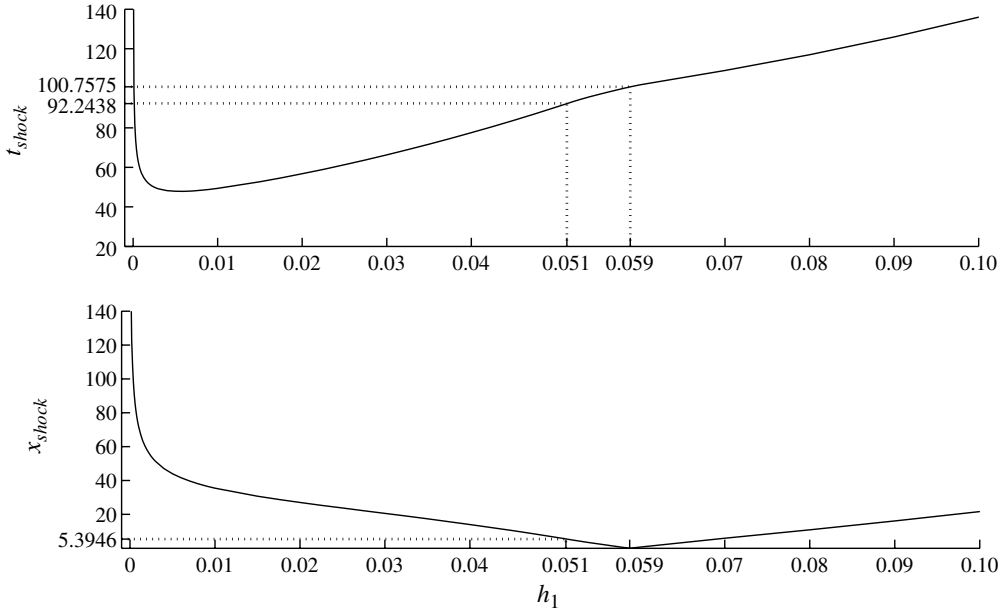
FIGURE 13. The time and position of the formation of the internal shock as functions of the dimensionless tailwater height. The dotted lines indicate the transitions of the location of the shock between different boundaries in the characteristic plane.

From this expression, we can calculate by numerical root finding the value of β at which $\partial t / \partial \alpha |_{\alpha = -\beta_m} = 0$ and hence from (5.6) and (5.7) we can find the time and position of the formation of the internal shock.

Figure 13 shows the time and position of the formation of the internal shock. We see that as $h_1 \to 0$, $t_{shock} \to \infty$ and $x_{shock} \to \infty$. This is the anticipated behaviour as we have shown above in the limit of no tailwater that the front speed is not diminished because reflected characteristics do not catch up with it. The time of the shock formation decreases as h_1 increases from 0 until it reaches a minimum time at $t = 47.8615$ for $h_1 = 0.006$. The time of shock formation increases monotonically for all tailwater heights after this minimum, passing continuously through the changes in boundary in the characteristic plane, indicated by the dotted lines in figure 13, until $t_{shock} \to \infty$ as $h_1 \to 1$. The position of the shock formation also decreases as h_1 increases from 0 until $h_1 = 0.0588$ when $x_{shock} = 0$. For $h_1 \geqslant 0.0588$, x_{shock} increases monotonically until $x_{shock} \to \infty$ as $h_1 \to 1$.

Physically, internal shocks will form when a region of fluid moving at a higher velocity impacts on another region of fluid moving with a lesser velocity. Figure 14 depicts the height and velocity profiles for $h_1 = 0.02$ at the time of internal shock formation $t = t_{shock} = 56.7777$. This is an example of the shock forming at the boundary between C_2 and S_2 at $x = x_{shock} = 27.0336$. We can see that the formation of the shock is due to the fluid in S_2 ($x < x_{shock}$) being of shallower height and moving faster than the fluid adjacent to it in C_2 ($x > x_{shock}$). Figure 15 shows the height and velocity profiles for $h_1 = 0.055$ at $t = t_{shock} = 96.8122$. This is an example of the shock forming at the boundary between U_2 and S_3 at $x = x_{shock} = 2.6556$. We can see that the formation of the shock is due to the fluid in U_2 ($x < x_{shock}$) being of shallower height than the fluid adjacent to it in S_3 ($x > x_{shock}$) and the fluid in S_3 moving with negative velocity against the motionless fluid in U_2. The height and velocity profiles at the time
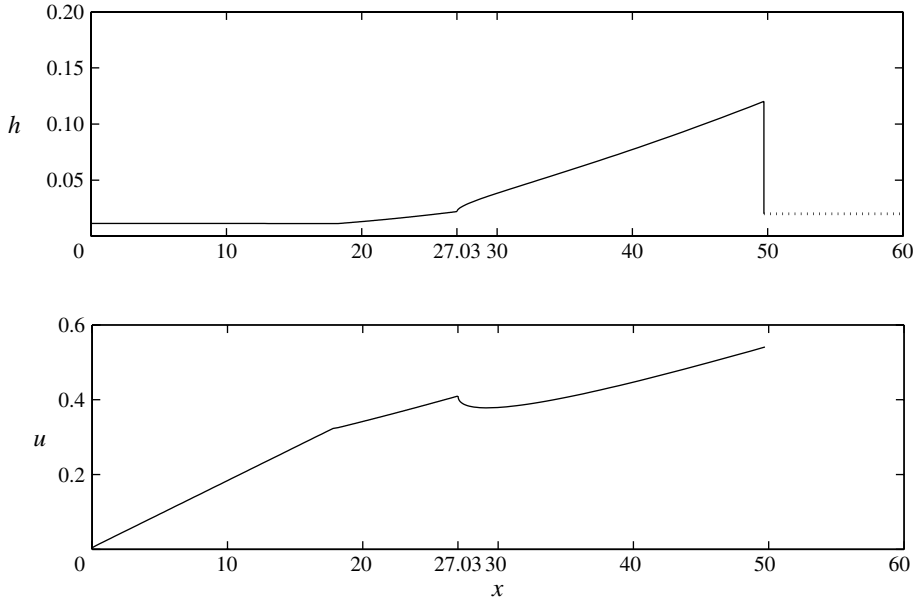
FIGURE 14. The height, $h(x, t)$, and velocity, $u(x, t)$, as functions of distance for $h_1 = 0.02$ at $t = t_{shock} = 56.7777$. The shock forms at the boundary between C_2 and S_2 at $x = x_{shock} = 27.0336$.
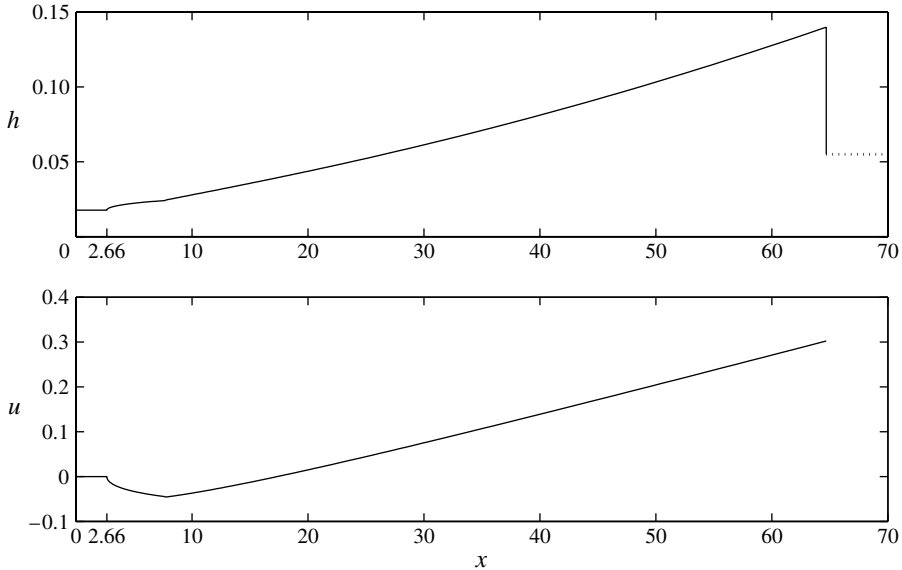
FIGURE 15. The height, $h(x, t)$, and velocity, $u(x, t)$, as functions of distance for $h_1 = 0.055$ at $t = t_{shock} = 96.8122$. The shock forms at the boundary between U_2 and S_3 at $x = x_{shock} = 2.6556$.

of shock formation are also shown in figures 11 and 12 at $t = t_{shock} = 135.9647$ for $h_1 = 0.1$. These are an example of the shock forming at the boundary between C_3 and S_3 at $x = x_{shock} = 21.6747$. We can see that the formation of the shock is due to

the fluid in C_3 ($x < x_{shock}$) being of larger height than the fluid adjacent to it in U_3 ($x > x_{shock}$) from figure 11, with $|u|$ being greater in U_3 than in C_3 from figure 12.

7. Summary and conclusions

The shallow-water equations have been used to model the flow of a finite volume of fluid instantaneously released from behind a lockgate onto a wet plane. Through the deployment of a hodograph transformation and Riemann's method, results are found using analytical techniques and, where necessary, simple numerical evaluations and quadrature. Our analysis has revealed three features of the dam-break motion that were previously unreported. These are that the front decelerates, the internal velocity becomes negative and that internal shocks form at later times.

The gravitational collapse of a reservoir of infinite extent into a tailwater was analysed by Stoker (1957). He demonstrated the motion, modelled using the shallow water equations, was governed by an expansion fan of characteristics centred at the front of the lock and the imposition of shock conditions at the front of the motion. For a finite reservoir, we have established that the presence of the wall at the rear of the dam causes initially rearward characteristics to be reflected, which significantly alters the solution and causes a complex wave region C_1 to form by the wall. For tailwater heights $h_1 < 0.0275$ we find that the complex region at the rear of the motion remains unbounded for all times whereas for $h_1 > 0.0275$ this complex region is bounded and a uniform region U_3 develops at later times adjacent to the wall in which there is no motion and a depth less than that of the tailwater. For all tailwater depths the reflected characteristics from the rear wall leave the complex region and travel across the released fluid to meet the front of the moving fluid, causing the height and velocity of the front to decrease (see figure 6).

For $h_1 > 0.0275$ the reflected characteristics from the rear wall all travel across the fluid and meet the front of the motion where they are reflected again. After being reflecting from the front they precede to travel back towards the rear of the dam, and a simple wave region is formed in which the velocity is negative (see figure 12). Once the characteristics meet the rear wall they are reflected again but stay localized to the rear wall in another region of negative velocity. Hence, there are three regions of motion at all times after the reflected characteristics from the front have met the rear wall (see figure 8). For $h_1 < 0.0275$ the reflected characteristics from the front do not travel back across the fluid to meet the rear wall and stay localized to the front and there are three regions of motion for all ensuing times with two complex wave regions either side of a simple wave region (see figure 7).

For all tailwater heights we find that after a period that we have calculated the hodograph transformation breaks down due to the intersection of characteristics and an internal shock forms. The location of these incipient internal shocks is found on three boundaries: the boundary between C_2 and S_2 for $h_1 \leqslant 0.0513$; the boundary between U_2 and S_3 for $0.0513 < h_1 < 0.0588$; and the boundary between C_3 and S_3 for $h_1 \geqslant 0.0588$ (see figure 13). The earliest time at which the solution breaks down is found to be $t = 47.8615$ which occurs for $h_1 = 0.006$.

Jánosi *et al.* (2004) conducted experiments of dam-break flows of a finite reservoir into a tailwater using a channel of length 993 cm with a lock of length 38 cm. Figure 16 shows a comparison of the front position of the flow between our analytical solution and data from Jánosi *et al.* (2004) in dimensional units with $\tilde{h}_0 = 15$ cm, $\tilde{h}_1 = 0.5$ cm and $\tilde{x}_0 = 38$ cm. We see that the analytical solution agrees well at early times and notably captures the time and position at which the reflected characteristics
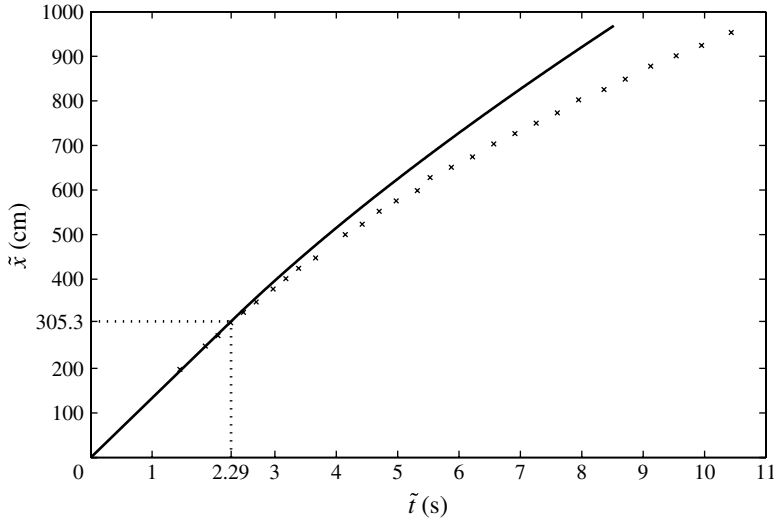
FIGURE 16. The dimensional position of the front of the flow as a function of time for a tailwater of dimensionless height 0.033 (—) plotted with data (×) from Jánosi *et al.* (2004). The front of the flow is decelerated by reflected characteristics from the rear wall after $\tilde{t} = 2.287$ s at $\tilde{x} = 305.3$ cm, indicated by the dotted line.

from the rear wall first decelerate the front at $(\tilde{x}, \tilde{t}) = (305.3 \text{ cm}, 2.287 \text{ s})$. We note that at later times the agreement is not as good and we postulate that drag from the sidewalls is further decelerating the flow and causing the divergence from our analytical solution. Jánosi *et al.* (2004) also present a data collapse of the temporal evolution of the front position of the flow; by plotting $\tilde{x}_s/\tilde{h}_0^{0.45}$ against $\tilde{t}$, they find that all of their data follow approximately the same curve. Such an empirical scaling is not consistent with the analysis in this paper. At early times we find that $\tilde{x}_s/(g\tilde{h}_0^{1/2})$ grows linearly with time, $\tilde{t}$, but that the constant of proportionality is dependent on the tailwater depth. This relationship established by Stoker (1957) is borne out by the experiments reported in Stansby *et al.* (1998) and Leal *et al.* (2006). Further, the data collapse of Jánosi *et al.* (2004) implies that the location at which the velocity of front of the flow is decelerated after the initial phase of motion is independent of the dimensionless tailwater depth. This is not in accordance with the results presented in this study in which the dimensionless height of the tailwater strongly influences the dynamics. The experiments of Jánosi *et al.* (2004) conducted for the data collapse had dimensionless tailwater depths within the narrow interval of (0.022–0.045) and thus some similarity between the different experiments is perhaps expected. We thus assert that a wider range of dimensionless tailwater depths must be considered to confirm the results presented within this study.

We conclude by observing that our results that have catalogued the various new phenomena have revealed how the presence of the tailwater strongly affects the flow and that a much richer range of dynamics emerge than for bounded dam-break flows into initially dry regions. The hodograph transformation and our analytical solutions allow us to pinpoint accurately the transitions between the various regimes. We note that because the results are not derived by the direct numerical integration of the primitive governing partial differential equations that they form an important test case against which the numerical results can be tested. Indeed the new analytical solutions

feature locations in which there are discontinuities in the dependent variables, or their gradients, and these provide a severe test for many numerical algorithms. Our results also reveal that the commonly used numerical practice of providing a shallow tailwater to study dam-break flows into initially dry regions may not capture accurately the detailed mechanics of the motion. Not only does the initial shock speed deviate from its dry bed case by a factor proportional to $h_1^{1/4}$, but also the presence of a tailwater inevitably introduces frontal deceleration and internal shock formation after a sufficient time.

Appendix

In this appendix we state explicitly the form of $\partial t/\partial \beta|_{\beta=\beta_m}$ on the boundary between C_2 and S_2. Internal shocks are found to form at this boundary when two β-characteristics coincide. To find the location at which this occurs on the boundary between C_2 and S_2, we are required to find the value of α for which $\partial t/\partial \beta|_{\beta=\beta_m} = 0$. The time field on this boundary is given by (4.13), and thus differentiating this expression with respect to β and setting $\beta = \beta_m$ we have

$$
\begin{aligned}
\left.\frac{\partial t(\alpha, \beta_s)}{\partial \beta_s}\right|_{\beta_s=\beta_m} &= t_2(2)\frac{3(6 + \beta_m - 4s)(6 - \alpha - 2\beta_m)}{8(2 - \beta_m)^{1/2}(\alpha - \beta_m)^{5/2}} \\
&+ \left(\frac{\partial t(2, \beta_m)}{\partial \beta_s} + \alpha_s'\frac{\partial t(2, \beta_m)}{\partial \alpha_s}\right)\frac{(2 - \beta_m)^{1/2}(4s - 2 - 3\beta_m)}{2(\alpha - \beta_m)^{3/2}} \\
&+ t_2(2)\frac{3(4s - 2 - 3\beta_m)((\alpha - \beta_m)(\alpha_s' - 1) + 1)}{4(2 - \beta_m)^{1/2}(\alpha - \beta_m)^{5/2}} \\
&+ t_2(2)\frac{2(\alpha_s'(\beta_m - s) + s - 2)}{(\alpha - \beta_m)^{3/2}(2 - \beta_m)^{1/2}} \\
&+ t_2(2)\frac{2(2 - \beta_m)^{1/2}(\alpha_s' - 1)}{(\alpha - \beta_m)^{3/2}}\left.\frac{\mathrm{d}s(\sigma)}{\mathrm{d}\sigma}\right|_{\sigma=2-\beta_m} \\
&+ \int_2^\alpha \frac{(a - \beta_m)^{3/2}}{(\alpha - \beta_m)^{3/2}}\left(\frac{3t_2}{2(a - \beta_m)} + \frac{\partial t_2}{\partial a}\right)\mathrm{d}a \\
&+ (\alpha_s' - 1)t_2(2)\frac{(2 - \beta_m)^{1/2}}{(\alpha - \beta_m)^{3/2}} \\
&\times \left(\frac{3(\alpha - 2)}{8(\alpha - \beta_m)}\left(\frac{1}{2} - \frac{2s - 2 - \beta_m}{2 - \beta_m}\left.\frac{\mathrm{d}\lambda(\sigma)}{\mathrm{d}\sigma}\right|_{\sigma=2-\beta_m}\right)\right. \\
&+ (6 + \alpha - 4\beta_m)\left(\frac{1}{2}\left.\frac{\mathrm{d}\lambda(\sigma)}{\mathrm{d}\sigma}\right|_{\sigma=2-\beta_m} - \frac{2s - 2 - \beta_m}{2 - \beta_m}\right) \\
&\left.- 2\left.\frac{\mathrm{d}s(\sigma)}{\mathrm{d}\sigma}\right|_{\sigma=2-\beta_m}\right),
\end{aligned}
\tag{A 1}
$$

where $\alpha_s' \equiv \partial \alpha_s/\partial \beta_s$.

REFERENCES

ANCEY, C., IVERSON, R. M., RENTSCHLER, M. & DENLINGER, R. P. 2008 An exact solution for ideal dam-break floods on steep slopes. *Water Resour. Res.* **44** (1).

ANTUONO, M. & HOGG, A. J. 2009 Run-up and backwash bore formation from dam-break flow on an inclined plane. *J. Fluid Mech.* **640**, 151–164.

ANTUONO, M., HOGG, A. J. & BROCCHINI, M. 2009 The early stages of shallow flows in an inclined flume. *J. Fluid Mech.* **633**, 285–309.

ARFKEN, G. B. & WEBER, H. J. 1995 *Mathematical Methods for Physicists*, 4th edn. Academic.

CARRIER, G. F. & GREENSPAN, H. P. 1957 Water waves of finite amplitude on a sloping beach. *J. Fluid Mech.* **4**, 97–109.

CARRIER, G. F., WU, T. T. & YEH, H. 2003 Tsunami run-up and draw-down on a plane beach. *J. Fluid Mech.* **475**, 79–99.

DRESSLER, R. F. 1958 Unsteady nonlinear waves in sloping channels. *Proc. R. Soc. Lond. Ser.* A 186–198.

ENSERINK, M. 2010 After red mud flood, scientists try to halt wave of fear and rumors. *Science* **330** (6003), 432.

FAVRE, H. 1935 *Etude Théorique et Expérimental des Ondes de Translation dans les Canaux Découverts (Theoretical and Experimental Study of Travelling Surges in Open Channels)*. Dunod, (in French).

GARABEDIAN, P. R. 1986 *Partial Differential Equations*. Chelsea Publishing.

HE, X. Y., WANG, Z. Y. & HUANG, J. C. 2008 Temporal and spatial distribution of dam failure events in China. *Intl J. Sedim. Res.* **23** (4), 398–405.

HOGG, A. J. 2006 Lock-release gravity currents and dam-break flows. *J. Fluid Mech.* **569**, 61–87.

HOGG, A. J., BALDOCK, T. E. & PRITCHARD, D. 2010 Overtopping a truncated planar beach. *J. Fluid Mech.* 1–33.

JÁNOSI, I. M., JAN, D., SZABÓ, K. G. & TÉL, T. 2004 Turbulent drag reduction in dam-break flows. *Exp. Fluids* **37** (2), 219–229.

KERSWELL, R. R. 2005 Dam break with Coulomb friction: a model for granular slumping? *Phys. Fluids* **17**, 057101.

LEAL, J. G. A. B., FERREIRA, R. M. L. & CARDOSO, A. H. 2006 Dam-break wave-front celerity. *J. Hydraul. Engng* **132**, 69.

MACCHIONE, F. & MORELLI, M. A. 2003 Practical aspects in comparing shock-capturing schemes for dam break problems. *J. Hydraul. Engng* **129**, 187.

PEREGRINE, D. H. 1966 Calculations of the development of an undular bore. *J. Fluid Mech.* **25** (02), 321–330.

PEREGRINE, D. H. 1971 Equations for water waves and the approximation behind them. In *Waves on Beaches and Resulting Sediment Transport: Proceedings of an Advanced Seminar Conducted by the Mathematics Research Center, the University of Wisconsin, and the Coastal Engineering Research Center, US Army, Madison, WI, 11–13 October 1971*, p. 95. Academic.

PRITCHARD, D., GUARD, P. A. & BALDOCK, T. E. 2008 An analytical model for bore-driven run-up. *J. Fluid Mech.* **610**, 183–193.

RITTER, A. 1892 Die fortpflanzung der wasserwellen. *Z. Verein. Deutsch. Ing.* **36** (2), 33.

SHIGEMATSU, T., LIU, P. L. F. & ODA, K. 2004 Numerical modeling of the initial stages of dam-break waves. *J. Hydraul. Res.* **42** (2), 183–195.

SOARES FRAZAO, S. & ZECH, Y. 2002 Undular bores and secondary waves-experiments and hybrid finite-volume modelling. *J. Hydraul. Res.* **40** (1), 33–43.

STANSBY, P. K., CHEGINI, A. & BARNES, T. C. D. 1998 The initial stages of dam-break flow. *J. Fluid Mech.* **374** (1), 407–424.

STOKER, J. J. 1957 *Water Waves*. Wiley.

TRESKE, A. 1994 Undular bores (favre-waves) in open channels-experimental studies. *J. Hydraul. Res.* **32** (3), 355–370.

VALIANI, A., CALEFFI, V. & ZANNI, A. 2002 Case study: Malpasset dam-break simulation using a two-dimensional finite volume method. *J. Hydraul. Engng* **128**, 460.

WHITHAM, G. B. 1974 *Linear and Nonlinear Waves*. Wiley.

YOCHUM, S. E., GOERTZ, L. A. & JONES, P. H. 2008 Case study of the big bay dam failure: accuracy and comparison of breach predictions. *J. Hydraul. Engng* **134**, 1285.